

LASERS

PACS numbers: 42.55.Px; 42.60.Fc; 42.65.Re; 42.79.Sz
DOI: 10.1070/QE2010v040n09ABEH014370

Performance of an optical amplifier/modulator based on a diode laser

A.P. Bogatov, A.E. Drakin, N.V. D'yachkov

***Abstract*. The performed numerical simulation shows that the main parameter determining the performance of an optical amplifier/modulator is the stimulated-emission cross section (differential gain) in the active region. A cross section of $\sim 3 \times 10^{-15}$ cm^2, which is quite realistic for modern heterostructures with quantum-well active regions, may provide an amplifier/modulator performance sufficient for data transfer at a rate of ~ 20 Gbit s^{-1}.**

Keywords: *mobile optical communication, semiconductor optical amplifier/modulator, quantum-well heterostructures.*

1. Introduction

The up-to-date optical fibre communication channels have almost completely replaced microwave and rf channels in the applications related to high-speed data transfer. However, this mainly holds true for local (stationary) communications, whereas the devices for mobile high-speed optical communications are being actively developed.

In particular, there are significant efforts in forming optical communication channels in space for data transfer from satellites at near-Earth orbits to geostationary satellites with subsequent data transfer to ground-based stations. The potential advantages of optical communications in comparison with mobile microwave and rf communications have not been implemented in view of some specific features.

The first attempts to direct apply the scientific and technical solutions successfully used in optical fibre communication lines to mobile channels met a number of new problems (some of which cannot be solved technically). Many of these problems are of physical nature and, therefore, require additional study.

Indeed, optical fibre communication lines use lasers that operate in the spectral ranges near 1.3 and 1.5 μm and generally have an output power of about 10 mW. These spectral ranges are chosen to obtain minima of dispersion and optical loss in fibre, whereas the output power is almost always limited by the fibre optical nonlinearity. When light propagates in free space, these requirements are removed, but others arise, which are related to the light divergence and impossibility or difficulties of using repeaters. This means that an emitter must form high-intensity light beams with a divergence close to the diffraction limit. In other words, the angular brightness of these sources should be maximally possible for lasers of a given type.

This problem was considered previously for steady-state lasing in high-power lasers (see, for example, [1 – 4] and references therein), where powers of ~ 1 W and higher, with a beam divergence close to the diffraction limit, were obtained by applying a special cavity design. However, this result does not solve the problem, because the laser beam should be modulated to transfer data. Moreover, the modulation frequency should exceed several Gbit s^{-1} to make the channel data capacity sufficiently high for modern communications.

Currently, the problem of designing an emitter that would simultaneously be a high-brightness light source and modulate light beams in the GHz range has not been solved. The point is that direct modulation of the beam intensity using pump current modulation leads to a time-dependent laser operation regime, which gives rise to the following effects. First, the transverse single-mode operation is violated, as a result of which the divergence may exceed the diffraction limit several tens of times. Second, the emission spectrum contains many longitudinal modes, and its width exceeds the modulation frequency by several orders of magnitude. These are very undesirable effects, because an increase in the beam divergence reduces the distance at which data can be transferred, while spectral broadening decreases the communication data capacity with spectral channel contraction [wavelength division multiplexing (WDM) technologies].

A promising device for solving the problem of high-speed mobile optical communication is a combined optical emitter, which is schematically shown in Fig. 1. It includes a master optical carrier frequency oscillator (for example, a low-power single-frequency cw laser), whose radiation is introduced into an amplifier/modulator (which modulates the pump current by the information signal) and then is amplified at the output of an optical power amplifier, which operates in the constant-pump regime. The output amplifier can provide a fairly high power level, for example, in the multiwatt range. All these active circuit elements are laser diodes based on quantum-well heterostructures, which currently have the best emission characteristics. The combined emitter can be either a hybrid version with optical-fibre connections or a monolithic single-crystal chip, similar to that considered in [5, 6].

A.P. Bogatov, A.E. Drakin, N.V. D'yachkov P.N. Lebedev Physics Institute, Russian Academy of Sciences, Leninsky prosp. 53, 119991 Moscow, Russia; e-mail: bogatov@sci.lebedev.ru

Received 3 June 2010
Kvantovaya Elektronika **40** (9) 782 – 788 (2010)
Translated by Yu.P. Sin'kov

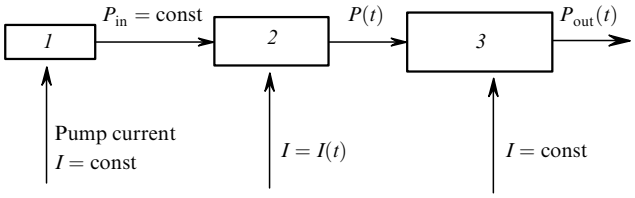

Figure 1. Simplified emitter scheme: (*1*) master oscillator, (*2*) amplifier/modulator, and (*3*) power amplifier.

Obviously, one of the key characteristics of this emitter is the amplifier/modulator performance. A diode laser based on a heterostructure with a bulk active region, operating in the regime of a single-frequency amplifier/modulator, was experimentally and theoretically studied in the early studies [7, 8]. A spectrally matched modulation was obtained, at which the optical spectrum width did not exceed the doubled modulation frequency. However, the upper limit of the modulation frequency was found to be as low as 2 GHz [7] and limited by the instrumental possibilities of the modulator. The amplifier/modulator was theoretically analysed in [8] in the quasi-steady-state approach, which does not make it possible to adequately estimate the upper limit of the modulation frequency.

In view of the aforesaid, it is interesting to analyse the performance of a diode amplifier/modulator with laser parameters characteristic of modern heterostructures with a quantum-size active region in order to determine the upper limit of its performance and the main parameters determining this limit.

2. Physical model and basic equations

The amplifier/modulator performance was simulated numerically. Note that analytical methods (for example, those used in [9]) can hardly be applied in this case, because the small-signal approximation is not quite correct under conditions of deep gain saturation.

The amplifier/modulator is a traveling wave amplifier with zero reflectances at the end faces. The transverse distribution of the propagating wave amplitude was assumed to be fixed and determined by the optical confinement factor Γ in the vertical direction (perpendicular to the plane of heterostructure layers) and the effective width W in the layer plane. The amplifier is pumped by a current I, which changes with time. This can be either a harmonic change according to the law

$$I(t) = I_0 + I_1 \sin(\Omega t), \quad \Omega = 2\pi v, \tag{1}$$

or a pulse-code modulation, for which the current can be written as

$$I(t) = \sum_{m=0}^{M} \xi_m f(t - mt), \tag{2}$$

where v is the modulation frequency; ξ_m is the data signal (a random function, which is, for example, either 0 or 1 at the mth step); and M is the total number of pulses per random process realisation. The function $f(t)$ is the form factor of the single pulse corresponding to this data signal. In the simplest case, this function can be expressed in terms of the Heaviside function $\theta(t)$:

$$f(t) = \theta(T/2 - |t|), \tag{3}$$

where T is the signal repetition period (inverse data transfer rate).

The model takes into account the spatially inhomogeneous inversion decay along the longitudinal amplifier axis z. A wave $E_0 \exp(-\mathrm{i}\omega_0 t)$ is incident on the left amplifier end face at $z = 0$ (Fig. 1). Its power, with allowance for the transverse beam size, can be written as

$$P_{in} = \frac{W d_a}{\Gamma} \frac{c n_{eff}}{8\pi} |E_0|^2, \tag{4}$$

where n_{eff} is the effective refractive index of the heterostructures and d_a is the active-region thickness.

The field inside the amplifier was presented as a traveling wave

$$\mathscr{E}(z,t) = E(z,t) \exp[\mathrm{i}(k_0 z - \omega_0 t)] \tag{5}$$

with a slowly varying complex amplitude $E(z,t)$ and $k_0^2 = \omega_0^2 \varepsilon(\omega_0)/c^2$, where $\varepsilon(\omega_0)$ is the spectral component of permittivity at the carrier frequency ω_0. The slow change in the amplitude $E(z,t)$ indicates that its spectral width Ω_E satisfies the inequality $\Omega_E \ll \omega_0$. It is assumed that, due to the change in the active-region inversion, the permittivity operator $\hat{\varepsilon}$ acquires a small additive

$$\Delta\varepsilon(t) = \delta\varepsilon(t) f_\varepsilon(\omega), \quad |\delta\varepsilon(t)| \ll \varepsilon(\omega_0), \tag{6}$$

where the form factor $f_\varepsilon(\omega)$ describes its dispersion.

Under the assumptions made the wave equation

$$\Delta\mathscr{E}(z,t) - \frac{1}{c^2} \frac{\partial^2 D(z,t)}{\partial t^2} = 0, \quad D(z,t) = \hat{\varepsilon}\,\mathscr{E}(z,t) \tag{7}$$

for a wave propagating in the amplifier, with allowance for the smallness of the above-mentioned parameters, is transformed into the following equation for the slow varying amplitude:

$$\frac{\partial E(z,t)}{\partial z} + \frac{n^*}{c} \frac{\partial E(z,t)}{\partial t} = \frac{\mathrm{i}\omega_0}{2cn} \delta\varepsilon(t) E(z,t), \tag{8}$$

where n^* is the group refractive index.

The expressions for the real and imaginary parts of the permittivity additive

$$\delta\varepsilon(t) = \Gamma(\mathrm{Re}\,\delta\varepsilon_a + \mathrm{i}\,\mathrm{Im}\,\delta\varepsilon_a), \tag{9}$$

where the subscript 'a' indicates the active region, were written conventionally:

$$\mathrm{Re}\,\delta\varepsilon_a = \frac{\partial \mathrm{Re}\,\varepsilon_a}{\partial N}\,\delta N = 2n_a \frac{\partial n_a}{\partial N}\delta N = 2n_a \Delta n_a(N), \tag{10a}$$

$$\mathrm{Im}\,\delta\varepsilon_a = -\frac{c n_a}{\omega_0}\, g(N). \tag{10b}$$

Here, n_a, $g(N)$, and N are, respectively, the refractive index, gain, and injected-carrier concentration in the active region. Thus, in our model, according to expressions (8)–(10), the dynamics of the amplitude $E(z,t)$ is set by the dynamics of the carrier concentration $N(t)$. The latter, in turn, is determined by the dynamics of change in the current and

carrier recombination rate, with allowance for stimulated recombination.

The calculations were performed on the assumption of linear concentration dependence of gain:

$$g(N) = \sigma(N - N_{\mathrm{tr}}), \tag{11}$$

where N_{tr} is the transparency concentration and σ is the stimulated-emission cross section (differential gain $\partial g/\partial N$). The derivative $\partial n_{\mathrm{a}}/\partial N$ was determined as a value proportional to σ, with allowance for the amplitude–phase coupling coefficient R. Representing the complex value $E(z,t)$ in the form

$$E(z,t) = E_{\mathrm{r}}(z,t)\exp[\mathrm{i}\varphi(z,t)], \tag{12}$$

we obtain the final system of equations describing the wave propagation in the amplifier:

$$\frac{\partial E_{\mathrm{r}}(z,t)}{\partial z} + \frac{n^*}{c}\frac{\partial E_{\mathrm{r}}(z,t)}{\partial t} = \Gamma\frac{g(N)}{2}E_{\mathrm{r}}(z,t), \tag{13a}$$

$$\frac{\partial \varphi(z,t)}{\partial z} + \frac{n^*}{c}\frac{\partial \varphi(z,t)}{\partial t} = \Gamma k_0 \Delta n_{\mathrm{a}}(N)\varphi(z,t). \tag{13b}$$

This system was solved simultaneously with the continuity equation for carriers in the active region

$$\frac{\partial N(z,t)}{\partial t} = \frac{I(t)}{WLd_{\mathrm{a}}e} - \frac{N(z,t)}{\tau} - \frac{cn_{\mathrm{a}}}{8\pi}\frac{g(N)}{\hbar\omega}E_{\mathrm{r}}^2(z,t), \tag{14}$$

where L is the amplifier length; τ is the injected carrier lifetime with respect to spontaneous recombination; and e is the elementary charge. The following initial and boundary conditions were used:

$$N(z,0) = N_{\mathrm{tr}}, \quad E_{\mathrm{r}}(z,0) = E_0, \quad \varphi(z,0) = 0, \tag{15a}$$

$$E_{\mathrm{r}}(0,t) = E_0, \quad \varphi(0,t) = 0. \tag{15b}$$

The calculations were performed numerically with time and space steps of 1 ps and 0.25 μm, respectively. As a result, the time dependences of the field power P and phase φ at the amplifier output were obtained. For a harmonic modulation of the current $I(t)$ these dependences took the form

$$P(t) = P_0 + P_1\sin(\Omega t - \psi), \tag{16}$$

$$\varphi(t) = \varphi_0 + \varphi_1\sin(\Omega t - \psi), \tag{17}$$

where ψ is the phase shift of the radiation power and field with respect to the pump current. For pulse-code modulation the output power and phase were calculated for a single pulse and a random sequence of M pulses (M is the 'word' length). In our calculations the M values did not exceed 60.

3. Model results and discussion

The values of the laser parameters used in the calculations are listed in Table 1. They are typical of modern laser diodes operating in the spectral range of 0.8–1.06 μm and based on heterostructures with a quantum-size active region. The parameters that were varied and differed from the basic values are indicated in Figs 2–9.

Table 1. Values of the basic laser parameters used in the calculations.

Designation	Parameter	Value
n_{a}	Refractive index of the active region	3.6
n_{eff}	Effective refractive index of the heterostructure	3.45
n^*	Group refractive index	3.9
τ	Spontaneous recombination time of carriers	1 ns
Γ	Optical confinement factor of heterostructure	0.0132
d_{a}	Active-region thickness	8 nm
W	Active-region width	3 μm
R	Amplitude–phase coupling coefficient	3
λ	Lasing wavelength	0.81 μm
α	Nonresonant absorption coefficient of heterostructure	20 cm^{-1}
σ	Stimulated-emission cross section	3×10^{-15} cm^2
L	Amplifier length	100 μm

The results corresponding to the amplifier pumping by a current modulated according to the harmonic law (1), with an amplitude $I_1 = I_0 = I$, are shown in Figs 2–6. These curves most clearly demonstrate the dynamic characteristics of the amplifier. Figures 2 and 3 show the dependences of the constant power component P_0, the amplitude of its variable component P_1, and the phase modulation amplitude φ_1 on the modulation current frequency. It can be seen that P_0 is almost independent of the modulation frequency in the range of 3–20 GHz. This is qualitatively clear, because in this range $\Omega\tau \gg 1$. Therefore, the time is too short for inversion to fall to the transparency threshold. The output power of the modulated component significantly decreases with an increase in the frequency (by a factor of 2–3) for low currents (50 mA) and only slightly decreases (by no more than 25 %) for currents above 100 mA in the frequency range from 0 to 15 GHz. This means that the modulation range, determined at a level of 3 dB, obviously exceeds 15 GHz. Note that the dependences of the modu-

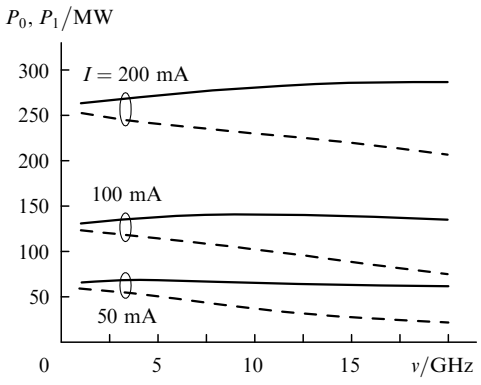

Figure 2. Dependences of the constant power component P_0 (solid lines) and power modulation amplitude P_1 (dashed lines) at the amplifier output on the modulating current frequency ν at different pump currents I and input light power $P_{\mathrm{in}} = 1$ mW.

lation bandwidth and signal power on the input signal are fairly weak. A change in the input signal power by a factor of 10 (from 1 to 10 mW) barely changes the characteristics of output radiation. The amplifier/modulator is insensitive to the input signal in this range, which is favourable for practice. The calculations showed also that the dependence of the modulated signal amplitude at a fixed frequency on the modulation current I is close to linear. This is completely consistent with the data [8], obtained within the simplified quasi-static model.

A specific feature of semiconductor lasers and amplifiers is the presence of amplitude–phase coupling, which manifests itself as follows: with a change in the inversion level (i.e., gain), the active-medium refractive index changes simultaneously and almost proportionally. This circumstance is reflected in Eqns (9) and (10) and in the calculation results presented in Fig. 3. One can see that the phase modulation bandwidth is close to the amplitude modulation bandwidth.

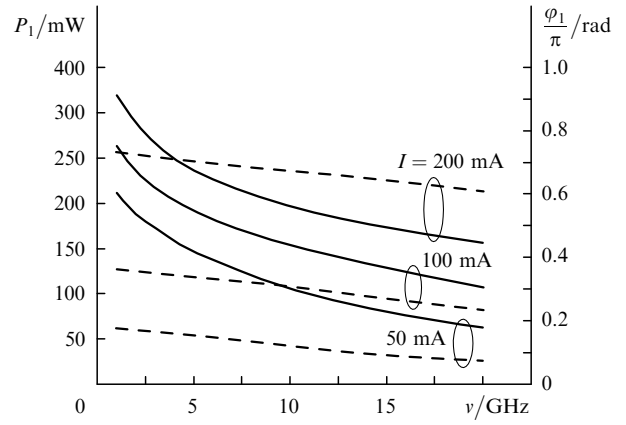

Figure 3. Dependences of the power modulation amplitude P_1 (dashed lines) and optical signal phase φ_1 (solid lines) on the modulation frequency ν at different pump currents I and power $P_{in} = 10$ mW.

The dynamic properties of the amplifier/modulator for different carrier lifetimes τ are shown in Fig. 4. It can be seen that the amplitude modulation depth is almost independent of τ. The spontaneous recombination time τ changes by an order of magnitude, whereas the modulation amplitude varies by no more than 7 %. This fact indicates that the parameter $\Omega\tau \gg 1$ is not effective. The frequency characteristic is determined by another characteristic parameter, specifically, the stimulated recombination time, which is inversely proportional to the stimulated-emission cross section.

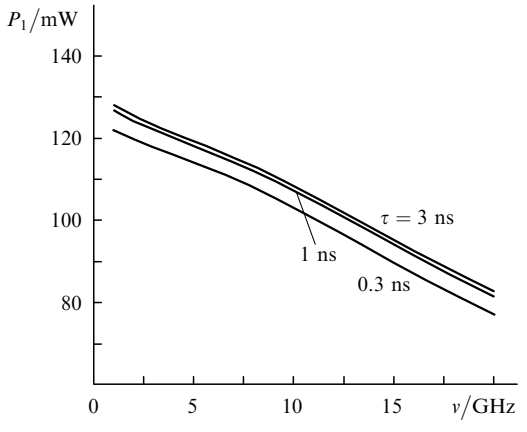

Figure 4. Dependences of the power modulation amplitude P_1 of optical signal on the frequency ν at different carrier lifetimes τ and power $P_{in} = 10$ mW.

Indeed, the calculations showed that the amplifier dynamic properties are primarily determined by the cross section σ (see Fig. 5).

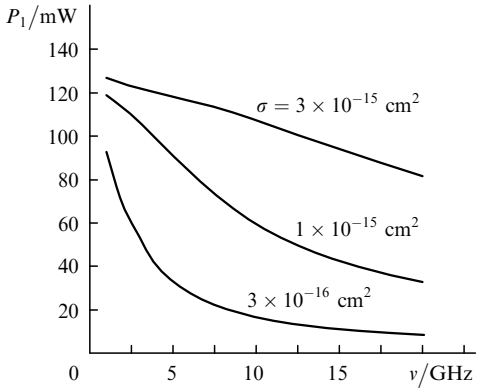

Figure 5. Dependences of the power modulation amplitude P_1 of optical signal on the frequency ν at different stimulated-emission cross sections σ and power $P_{in} = 10$ mW.

The choice of the amplifying diode length L is important from the practical point of view. The conditions for convenient matching of the electric output of integrated circuit with the current supply circuit determine the total current through the amplifier to be an invariant. In this case, the choice of the optimal amplifier length is not obvious. Indeed, a change in this parameter leads to two opposite effects. In particular, an increase in the amplifier length causes an increase in the total (per pass) optical amplification due to the increase in the optical path length. At the same time, the pump current density simultaneously decreases (with conservation of the total current through the amplifier); accordingly, the local gain decreases as well. Therefore, it is not clear beforehand to what extent one effect compensates for the other when the gain saturation is inhomogeneous over the cavity length.

In our model this problem could be solved using the data in Fig. 6. According to them, the effect caused by the increase in the pump current density is dominant for the amplitude component of modulation. The phase component is determined to a greater extent by the integral effect of phase incursion over the diode length. An analysis of the data in Fig. 6 suggests that the most favourable conditions for amplitude modulation are implemented at the minimum amplifier length. In turn, this means that the choice of the optimal length is determined by the compromise between the technological difficulties in producing small-size diodes with and possible gain due to the increase in modulation efficiency.

The results for harmonic modulation only qualitatively characterise the data transfer rate, because such a modulation cannot transfer any data. A more complete pattern can be obtained using a current subjected to pulse-code modulation (which is a quasi-random process).

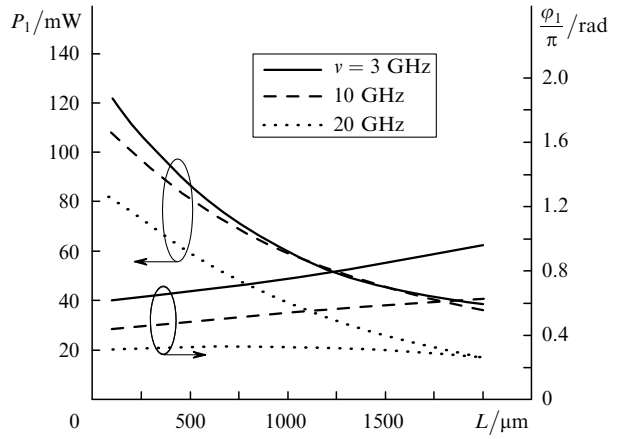

Figure 6. Dependences of the power modulation amplitude P_1 and phase φ_1 of optical signal on the amplifier/modulator length at different frequencies ν and power $P_{in} = 10$ mW.

Figures 7 shows the response functions for the power and phase shift of amplifier/modulator output radiation after applying a 50-ps rectangular current pulse. This pulse width can provide a data transfer rate of ~ 20 Gbit s^{-1}.

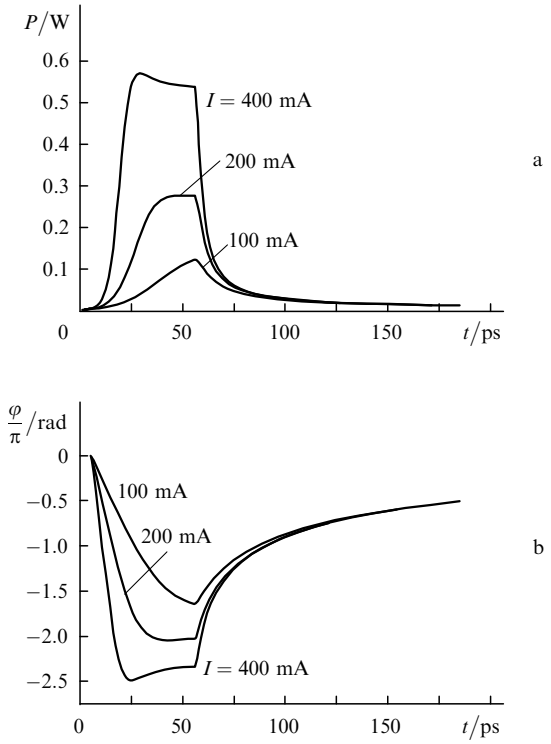

Figure 7. Response functions of the (a) power and (b) phase shift of the amplifier/modulator output radiation for 50-ps rectangular current pulses with different amplitudes I; $L = 100$ μm and $\sigma = 3 \times 10^{-15}$ cm^2.

These calculation data correspond to three current amplitudes. It can be seen that an increase in the current not only leads to an increase in the output power of the optical pulse but also changes its shape. This change is in essence a decrease in both the front and trailing edges. The physical nature of this behaviour is the decrease in the effective time of stimulated carrier recombination in the active region. Thus, the increase in the pump current amplitude is accompanied by not only an increase in the output pulse power but also an increase in the amplifier performance. This is in agreement with the data for the above-described harmonic current modulation (Figs 2, 3).

The amplifier/modulator performance for current pulses of the same amplitude but different widths is clearly illustrated by Fig. 8. At the amplifier parameters that were used in the calculation, a decrease in the pulse width below 50 ps is hardly expedient; i.e., the ultimate data transfer rate is limited by 20 Gbit s^{-1}. It is fairly difficult to increase the performance by increasing the current pulse amplitude (see above), which is limited by both the supply circuits of the amplifier and the electric parameters of the laser diode. There are always limitations on the rate of the current increase in supply circuits, for example, because of spurious inductances.

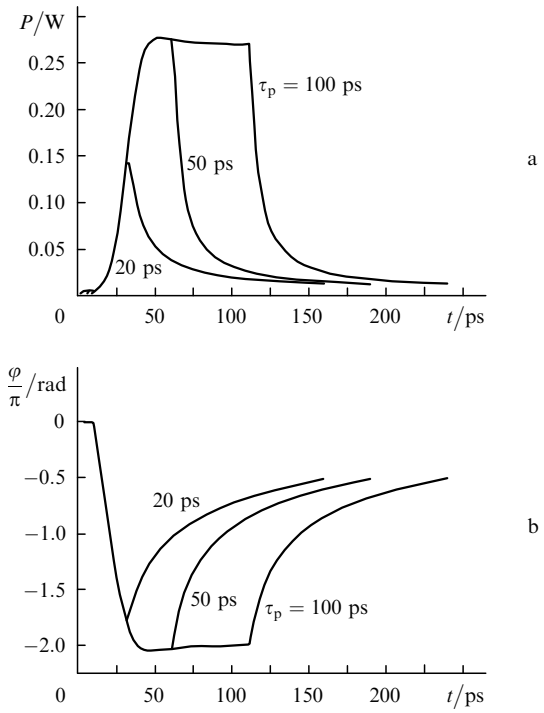

Figure 8. Response functions of the (a) power and (b) phase shift of the amplifier/modulator output radiation for rectangular current pulses with an amplitude of 200 mA and different widths τ_p; $L = 100$ μm and $\sigma = 3 \times 10^{-15}$ cm^2.

In this context, it is most interesting to obtain a higher performance using the internal laser amplifier parameters. The calculations showed that one of such parameters, which significantly affect the performance, is the stimulated-emission cross section σ. The data in Fig. 9 clearly demonstrate the dependence of the amplifier/modulator performance on σ. They are also in agreement with the results obtained for the harmonically modulated pump current (Fig. 5).

One of the main characteristics determining the data transfer rate is the bit error rate. It is most descriptively illustrated by the so-called eye diagram. In our case this diagram shows the shape of the signal at the amplifier output under pump current modulation by a large number of random sequences of pulses with amplitudes of 0 and 1 (information 'words') in a time window equidistantly spaced

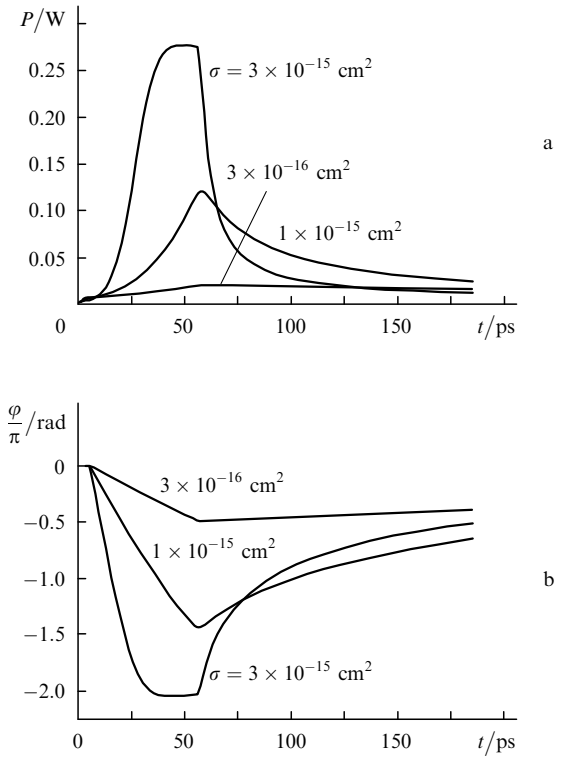

Figure 9. Response functions of the (a) power and (b) phase shift of the amplifier/modulator output radiation for 50-ps rectangular current pulses with an amplitude of 200 mA at different stimulated-emission cross sections σ and $L = 100$ μm.

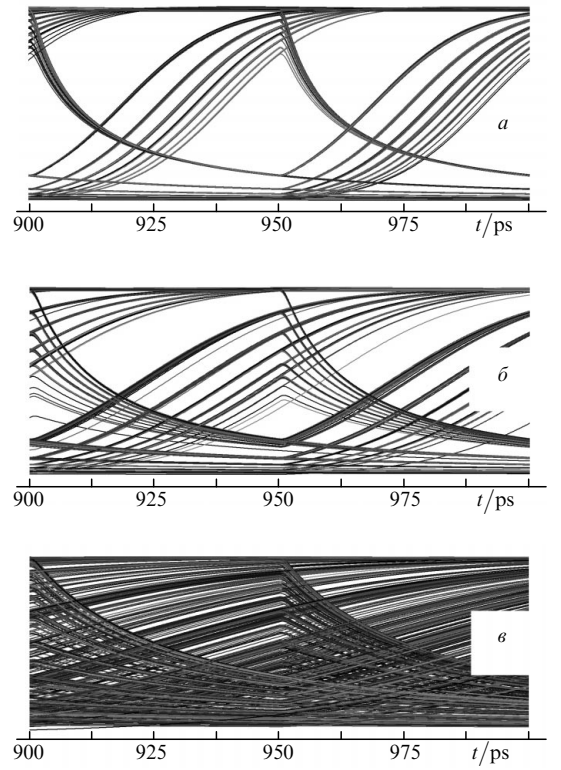

Figure 10. Eye diagrams of the amplifier/modulator under modulation by random sequences of 50-ps current pulses with an amplitude of 100 mA (length of one sequence 20 bit, number of random sequences 10^3) for stimulated-emission cross sections $\sigma =$ (a) 3×10^{-15}, (b) 2×10^{-15}, and (c) 1×10^{-15} cm^2. The last two bits are shown.

from the beginning of each 'word'. Figure 10 shows the results of modeling three such diagrams for the output signal (power) of an amplifier/modulator pumped by a current set by Eqns (2) and (3). This example shows that a cross section $\sigma = 3 \times 10^{-15}$ cm^2, which is characteristic of quantum-well active regions, allows for a mode in which the amplifier/modulator does not introduce additional communication errors at data transfer rates up to 20 Gbit s^{-1}. At the same time, if the cross section σ is below this value, the limiting data transfer rate (determined by σ) will be, correspondingly, smaller.

Similar eye diagrams can also be constructed for phase detection; however, they are omitted here because their specific form depends on the phase detection method. Nevertheless, it follows from Fig. 7 that the amplifier performance is approximately the same under amplitude and phase modulations.

4. Conclusions

The main results of this study are as follows.

(i) It was shown by numerical simulation that semiconductor heterostructures with a quantum-well active region, which have typical parameters and stimulated-emission cross section of $\sim 3 \times 10^{-15}$ cm^2 and designed to work in the spectral range of 0.8 – 1.06 μm, can be used to develop light amplifier/modulators with a modulation bandwidth up to 15 GHz at a level of 3 dB for data transfer at rates up to 20 Gbit s^{-1}.

(ii) The laser amplifier/modulator performs mixed amplitude – phase modulation. With a change in the amplifier operation regime (current amplitude, modulation frequency, etc.) the levels of amplitude and phase modulation change synchronously.

(iii) The stimulated-emission cross section was found to be the main internal parameter determining the performance and upper limit of modulation bandwidth.

Based on these results we can conclude that the proposed scheme for obtaining a modulated beam of diode laser radiation yields a performance not lower than the conventional method of direct modulation of diode laser current. However, in comparison with this method the scheme proposed has a number of significant advantages, in particular, the possibilities of implementing not only amplitude but also phase modulation and designing WDM systems with compaction close to the theoretical limit.

References

1. Mikula M. *Topics Appl. Phys.*, **78**, 265 (2000).
2. Sumpf B., Hulsewede R., Erbert G., Dzionk C., Frieke J., Knauer A., Pittroff W., Ressel P., Sebastian J., Wenzel H., Tränkle G. *Electron. Lett.*, **38**, 183 (2002).
3. Paschke K., Bogatov A.P., Drakin A.E., Güther R., Stratonnikov A.A., Wenzel B.H., Erbert G., Tränkle G. *IEEE J. Sel. Top. Quantum Electron.*, **9**, 835 (2003).
4. Paschke K., Bogatov A.P., Bugge F., Drakin A.E., Fricke J., Güther R., Stratonnikov A.A., Wenzel B.H., Erbert G., Tränkle G. *IEEE J. Sel. Top. Quantum Electron.*, **9**, 1172 (2003).
5. Kwok C.H., Penty R.V., White I.H., Hasler K.-H., Sumpf B., Erbert G. *IEEE Photon. Technol. Lett.*, **21**, 301 (2009).
6. Michel N., Ruiz M., Calligaro M., Robert Y., Lecomte M., Parilland O., Krakovski M., Esquivias I., Odriazola H., Tijero J.M.G., Kwok C.H., Penty R.V., White I.H. *Proc. SPIE Int. Soc. Opt. Eng.*, **7616**, 7616F (2010).

7. Annenkov D.M., Bogatov A.P., Eliseev P.G., Okhotnikov O.G., Pak G.T., Rakhval'skii M.P., Fedorov Yu.F., Khairetdinov K.A. *Kvantovaya Elektron*., **11**, 231 (1984) [*Sov. J. Quantum Electron*., **14**, 163 (1984)].
8. Bogatov A.P. *Trudy FIAN*, **166**, 68 (1986).
9. Olshansky R., Hill P., Lanzisera V., Powazinik W. *IEEE J. Quantum. Electron*., **23**, 1410 (1987).